JOURNAL OF CATALYSIS 85, 405–414 (1984)

Supported PdPt Alloy Catalysts: Synthesis, Structure Characterization and Effects of Hydrogen Absorption

G. COCCO, G. CARTURAN, S. ENZO, AND L. SCHIFFINI

Facoltà di Chimica Industriale, Calle Larga S. Marta 2137, 30123 Venezia, Italy

Received May 17, 1983; revised August 8, 1983

Pd/Pt alloy catalysts were prepared by anchoring Pd(II) and Pt(II) organometallic species to the support surface, followed by H_2 reduction under mild conditions. This preparation method was exploited for the synthesis of Pd/Pt catalysts having different Pd/Pt ratios and with total metal loading ~2%; pure Pd and pure Pt catalysts were also obtained. Small Angle X-ray Scattering (SAXS) analysis was used to determine metal dispersion: average metal particle diameter was in the range 20–40 Å both for alloy and single Pd and Pt catalysts. The occurrence of Pd/Pt alloy formation was demonstrated by Wide Angle X-ray Scattering (WAXS) and Radial Distribution Function (RDF) analyses. Results both from WAXS and RDF are consistent with each other in ascertaining alloy occurrence, also providing a detailed picture of the behavior of Pt, Pd, and Pd/Pt systems in the presence of H_2.

INTRODUCTION

Bimetallic systems have recently been the subject of growing interest in catalysis (*1–3*). In particular, with bimetallic catalysts composed by alloying two group VIII metals, recent accounts describe a wide-ranging set of experiments concerning their preparation, characterization, and stability (*3–5*). The reactivity of these alloy catalysts has also been tested in isomerization (*6*), hydrogenolysis (*7*), deuterium exchange (*8*), and hydrogenation reactions (*9, 10*).

Non-supported Pd/Pt catalysts have also been used in selective hydrogenation of alkynes, where the Pd/Pt atomic ratio and extent of hydrogen absorption turned out to be the most important parameters affecting selectivity (*11*). Along this line, it seemed interesting to cover this topic in the specific case of highly dispersed Pd/Pt alloys, since we had already shown the effective role of metal dispersion in determining selectivity (*12*).

Two main problems must immediately be taken into account in approaching this subject properly.

First, at variance with the preparation of alloy films from the vapor phase, the synthesis of highly divided alloy catalysts is not a straightforward chemical process. Ordinary methods, such as reduction of mixed salts impregnated on the support, do not guarantee the formation of alloy phases (*13, 14*); in many cases the drastic experimental operations may induce extensive sintering (*15, 16*). Previous experiments in preparing catalysts on vitreous materials starting from the corresponding organometallic precursors (*12, 17*) suggested that the same procedure should be used to obtain bimetallic catalysts.

Thus, we attempted the synthesis of highly dispersed Pd/Pt alloys by reacting Pd and Pt allyl derivatives with surface —OH groups of supports and then reducing the two anchored allyl species with H_2. The results are presented in this paper.

The second point concerns the unambiguous characterization of the alloy phase formation. Chemisorption analysis may result in questionable data, particularly in the case of Pd/Pt alloys; transmission electron microscopy may be not useful in testing alloy occurrence and only allows the

0021-9517/84 $3.00

examination of a small volume of the sample. Moreover, the close overlapping of the independent Pd and Pt diffraction lines reduces the effectiveness of X-ray scattering methods in the characterization of a Pd/Pt alloy. Nevertheless, the property of Pd metal to generate βPdH under H_2 (*18, 19*), displaying a characteristic X-ray pattern, may offer an opportunity to demonstrate the occurrence of Pd species possibly not alloyed with Pt. Accordingly, an X-ray investigation was carried out "*in situ*" under H_2 on several Pd/Pt catalysts over a broad range of compositions. Moreover, owing to the strong smearing effects on the conventional diffraction patterns due to particle dispersion, Radial Distribution Function (RDF) analysis also seemed well suited to the problem. Some of the results were also checked by Small Angle X-ray Scattering (SAXS).

The method followed also allows a concurrent study of the intrinsic reactivity and general behavior of Pd/Pt alloys vs H_2—an important parameter, since the ultimate goal of our investigation was the use of these Pd/Pt catalysts for hydrogenation reactions.

EXPERIMENTAL

Catalyst preparations. All chemicals used were analytical grade products; solvents were dried and distilled before use. The working techniques for air-sensitive compounds were used throughout all experiments involving preparation and handling of catalysts.

The $SiO_2/Al_2O_3/Na_2O$ = 71/18/11 support was prepared according to the reported procedure (*20*). Pd, Pt, and Pd/Pt dispersions were obtained by reacting a stirred pentane suspension of the powdered support with pentane solutions of Pd $(C_2H_5)_2$, $Pt(C_3H_5)_2$, or $Pd(C_3H_5)_2$ + $Pt(C_3H_5)_2$, respectively, at 0°C. One milliliter of pentane/g of support ratio = 1 was used. Allyl species concentrations ranged in the interval 0.07–0.09 *M*; appropriated volumes of these solutions were used in order to adjust the total metal loading to ~2% in support weight.

The reaction involves the anchoring of the organometallic species to the support —OH groups and occurs with propene evolution (*17*). GLC analysis of the gas phase confirmed the occurrence of this reaction, which was completed in about 1 h. After this time the solution was colorless and the stirred suspension was reacted with H_2 at −10°C. Progressive formation of dispersed metal was shown by changes in the support color which turned from buff to black–gray. The solvent was evaporated under reduced pressure and the catalysts obtained were stored in an inert atmosphere. Typically 20–30 g crops of catalyst were prepared for each sample.

X-Ray analysis. Our experimental procedures and raw data reduction and analysis have repeatedly been described in our recent papers (*17, 21, 22*). Some supplementary details are given below, together with a short definition of the terms employed.

The wide-angle scattered intensities were collected in the reflection geometry with a fully automatic horizontal diffractometer connected to a highly stabilized generator. Soller slits, a graphite focusing crystal as a monochromator, and a scintillation counter fitted with a pulse analyser were employed. A special steel sample-mounting X-ray camera and a suitable sample-holder attachment were developed (*19*).

Two sets of experiments were performed. Ni-filtered Cu$K\alpha$ radiation was first used and the samples were step-scanned across the 111 and 200 Pd reflection range by 0.02° steps in 2θ, 2θ being the scattering angle, provided that 4×10^4 counts per point were accumulated. Then H_2 was admitted into the thermostatic sample cell, flow rate being typically 30 ml/min, and the peak shifts were observed.

X-Ray data for radial distribution analysis was taken using Zr-filtered Mo$K\alpha$ radiation in the preset count mode from $\theta = 2°$ to $\theta = 62°$, corresponding to the range $0.5 < h < 15.3$ Å^{-1} ($h = 4\pi \sin\theta/\lambda$ and λ = X-ray

wave length). Several runs were taken to accumulate 10^5 counts; intensities were averaged and corrected for background, polarization and absorption. Above $2\theta = 70°$ intensity data were smoothed with a least-squares cubic splines algorithm to remove irregularities due to statistical uncertainties at larger angles. The corrected intensities, converted from 2θ to h, were reduced to absolute units, $I_{eu}(h)$, using the analytical method of KroghMoe (*23*) and visual comparison. The atomic scattering factors proposed by Cromer and Mann (*24*), which were corrected for anomalous dispersion, and the Compton scattering factors of Smith *et al.* and Palinkas *et al.* were employed (*25*).

A scattering function $i(h)$ was then evaluated according to the specific definition of Pings and Waser (*26*):

$$i(h) = \left(I_{eu}(h) - \sum_{j=1}^{m} x_j f_j^2\right) \Big/ \left(\sum_{j=1}^{m} x_j f_j\right)^2 \quad (1)$$

where f_j are the atomic scattering factors corrected for anomalous dispersion and x_j the stoichiometric coefficients of a hypothetical structural unit containing m kinds of atoms.

The so-called reduced atomic distribution function $Q(r)$ was obtained from $i(h)$ by Fourier transform according to

$$Q(r) = 4\pi r[\rho(r) - \rho_0] = \frac{2}{\pi} \int_{h_{min}}^{h_{max}} hi(h)\sin hr \, dr \quad (2)$$

where ρ_0 is the average atomic density of the scattering system, $\rho(r)$ the weighted radial density function, and h_{min}, h_{max} the lower and upper limits of the experimental intensities.

SAXS measurements were carried out with a Kratky compact camera by following the procedure already reported (*17*). Zr-filtered Mo$K\alpha$ radiation with a pulse-height discriminator and a scintillation detector were used. The metal particle surface areas were obtained from the asymptotic behavior in the wings of small-angle intensities after subtracting the background and matrix effects according to the basic equation:

$$S_{sp} = \frac{16\pi^2 \lim_{m\to\infty} m^3 J(m)}{a^2 \lambda^4 r_e^2 N_A P_0 (\Delta\rho)^2 p} \quad (3)$$

where m is the instrumental variable (μm), $J(m)$ is the slit-smeared intensity (n_e^2 cps cm^{-1}, n_e = number of electrons, and cps = counts per second); r_e^2 is the Thompson factor (cm^2); N_A the Avogadro number; P_0 the energy per cm of length of the primary beam weakened by the scattering sample (*27*); p is the sample thickness obtained by multiplying sample concentration (g cm^{-3}) by the sample holder thickness (cm); a is the distance between the sample and the recording plane (cm): complete Pd/Pt alloying was assumed for the calculation of the difference between the mean electronic density of the metal particles and matrix ($\Delta\rho$).

RESULTS

The analytical data of the catalysts examined are listed in Table 1.

A preliminary experiment to test the effectiveness of X-ray analysis was performed on a sample prepared by mechanically mixing the support with the appropriate amounts of Al 100 and A 100 catalysts to achieve a Pt/Pd atomic ratio of 0.25 and a total metal loading of 1.2 wt%. The relevant diffraction patterns observed with or without H_2 fluxing are shown in Fig. 1. The 111 peaks (or the 200 ones) of Pd and Pt overlap in the absence of H_2 (broken line), whereas they clearly split under H_2 (dotted line), revealing two well-separated phases: the Pt diffraction lines still persist at approximately original positions, whereas two new peaks appear at 39.88 and 46.45°, respectively, easily assignable to the β PdH phase.

We briefly mention here that the lattice structure of palladium hydrides represents a coherent isotropically expanded form of fcc Pd lattice, the hydrogen atoms lying interstitially in the octahedral sites. In the region of small hydrogen solubilities, the

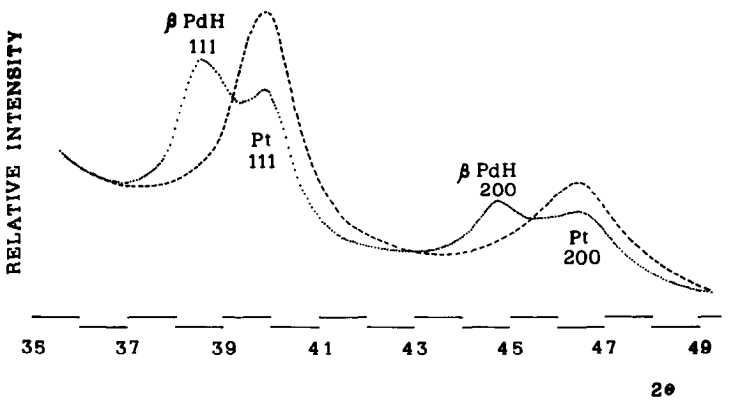

FIG. 1. X-Ray diffraction profiles of 111 and 200 peaks from a mechanical mixture of Pd + Pt catalysts (broken line). The overlapping reflections split under H_2 fluxing (dotted line) showing the occurrence of β PdH, whereas unaffected Pt crystallites hold their own line positions.

solid solution is designated as α phase and exists in the original metal lattice; a second hydrogen-rich non-stoichiometric phase, called β, exhibits a significant lattice expansion vs hydrogen content. At room temperature the values of the fcc lattice constants for α (limiting upper composition $PdH_{0.015}$), and β (lower limit $PdH_{0.607}$) phases are $a_{Pd\alpha}$ = 3.894 Å and $a_{Pd\beta}$ = 4.025 Å, respectively, compared with a pure palladium constant of 3.890 Å (*28, 29*).

Within this frame of reference the 4.05-Å lattice constant, although calculated only from the 39.88° and 46.45° peaks of Fig. 1, indicates conversion of the Pd particles into the β hydride phase beyond experimental uncertainty: the parameter obtained is in fact larger than that of $a_{Pd\beta}$ usually quoted for β PdH phase low boundary.

TABLE 1

Summary of Bimetallic Catalysts Investigated[a]

Catalyst[b]	Metal content, wt%		Metal phase composition, at%		Atomic ratio Pt/Pd
	Pd	Pt	Pd	Pt	
Al 00	1.45	—	100	—	0.00
Al 10	1.20	0.24	90.1	9.9	0.11
Al 13	2.8	0.95	87.2	12.8	0.15
Al 18	0.80	0.33	81.6	18.4	0.23
Al 31	0.70	0.60	69.8	31.1	0.45
Al 100	—	1.20	—	100	1.00

[a] All catalysts supported on the same xerogel.
[b] Catalyst symbol represents the values of Pt at% on the basis of atomic absorption analysis.

Different behavior was observed for the Pd/Pt alloy catalysts of Table 1. The diffraction patterns with and without H_2 fluxing are shown, as an example, in Fig. 2, which refers to catalyst Al 10. The entire peak areas belonging to the 111 and 200 Pd and Pt reflections (broken line) move under flowing H_2 toward smaller scattering angles; no splitting that could be assigned to distinct metallic phases was observed (dotted line). The absence of Pt diffraction peaks is of particular relevance and suggests that the entire metal loading is engaged in hydride phase formation. Thus, the behavior under H_2 of Al 10 catalyst (to which the remainder of samples comply) shows, although indirectly, the occurrence of Pd and Pt alloying.

It must be pointed out, however, that the peak shifts of 111 and 200 Pd/Pt reflections in alloy catalysts are reduced with respect to the corresponding shifts observed in the case of the Pd reflections in the examined Pd + Pt mechanical mixture: this is shown by the βPdH 111 line quoted as a reference in Fig. 2. As will be discussed later, this

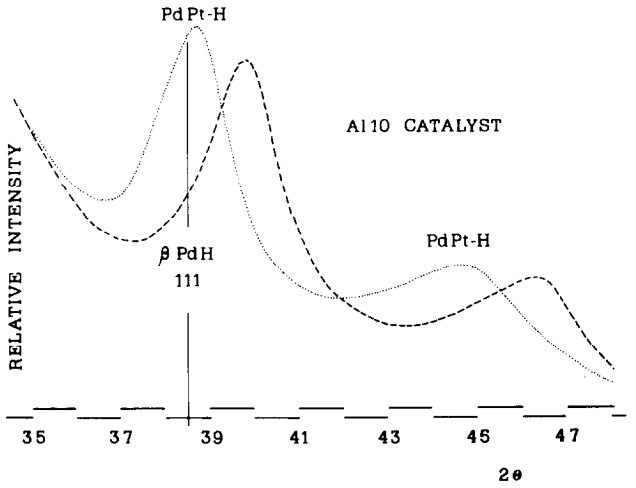

FIG. 2. X-Ray diffraction profiles of 111 and 200 peaks from Al 10 bimetallic catalyst (broken line). The lack of Pt reflections under H_2 fluxing is plainly recognizable (dotted curve) manifesting Pd/Pt alloying. The vertical line marks the β PdH 111 peak position.

reduction of shift is proportional to the Pt content in the alloy. In other words, under H_2 flow, a noticeable change of lattice spacing as a function of alloy composition may be surmised.

This suggested the possible correlation should be pursued further. In this connection, for additional information on the structural conditions of the hydride phases, we turned to RDF of atom analysis for all the catalysts listed in Table 1 as well as for the support. Indeed, in the absence of H_2 fluxing, changes in Pd lattice constant merely due to Pt allowing are not significant in substantiating the establishment of the alloy phase (30). Moreover, our approach may be a useful tool in avoiding general difficulties in determining lattice constants of highly divided metal arising, for example, from strong line broadening, absence of high-order reflections and line displacements due to strain effects, particularly at low scattering angles.

The angular intensity obtained directly from the experimental X-ray curve of catalyst Al 10, reduced to electron unit intensity and adjusted to total independent scattering, is reported in Fig. 3 as an example.

The reduced radial distribution functions $Q(r)$ are plotted in Fig. 4 (broken line), the catalyst codes being quoted in the inset. The upper curve refers to the support: it may be noted that the two main peaks at 1.65 and 3.2 Å, ascribed to Si—O and Si—Si nearest neighbor coordinations respectively, are close to the corresponding interactions in glasses of similar composition (*31*), in spite of the particular texture of the gel (specific surface area determined by

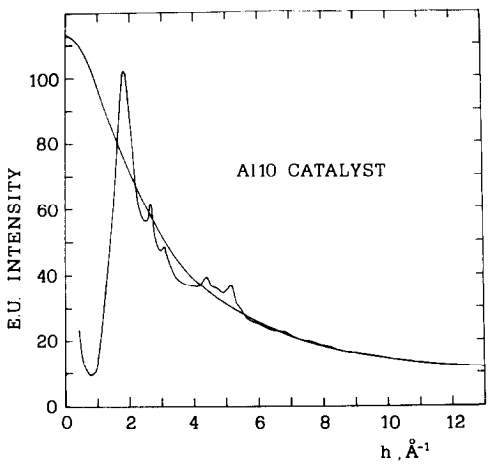

FIG. 3. Scattered intensity, adjusted and reduced to electron units from Al 10 catalyst. The calculated total intensity, free from interference effects, is also shown.

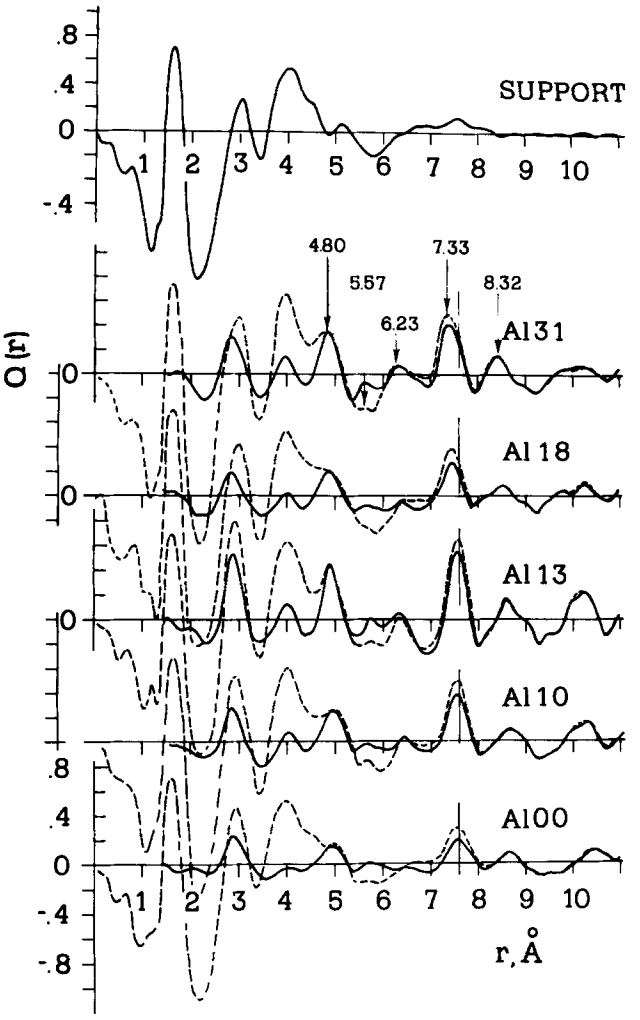

FIG. 4. Reduced radial distribution functions, $Q(r)$, for the support (upper curve) and catalysts (lower curve, dotted line) under H_2 fluxing. The differential $Q(r)$s obtained after subtracting the support contribution are presented as solid curves.

SAXS = 362 m^2/g; density = 1.98 g/cm^3). Although not resolved, the broad peak at about 4.2 Å is indicative of Si 2nd oxygen coordination shell; finally, after further modulation at about 5.2 Å, significant correlations rapidly fade away.

In the $Q(r)$ catalyst functions, resulting from sample examination under H_2 fluxing (Fig. 4; dashed lines), the peak at 1.65 Å appears imperturbed, whereas significant changes occur in the subsequent support-due coordination peaks. Particularly, superimposed on the shoulder of the third main maximum, a new feature is clearly discernible at around 5 Å. Moreover, high modulations occurring at greater distances and the presence of an important peak at about 7.5 Å clearly manifest the supported metallic phase. Even disregarding the shorter metal–metal distances overshadowed in detail, a general pattern may be deduced for all samples examined assignable to a fcc structured phase. For instance, when the higher correlation peaks for catalyst Al 31 are considered, the metrical distances (see Fig. 4) conveniently fit into a fcc

unit cell constant of 3.93 Å. Nevertheless, for the convenience of further considerations, difference radial functions have been reconstructed removing the support contribution from catalyst radial functions. Although somewhat questionable, this treatment was valuable bearing in mind that our main concern was to spot differences between the samples. Moreover, the conformity of the first radial peak in the xerogel and catalyst $Q(r)s$ (broken line), and the absence of spurious details in the difference functions (solid line) support our confidence in the adopted procedure. The resulting picture completes the above structural pattern, the nearest-neighbor metal–metal interactions r_1 and the fcc $r_1\sqrt{2}$ distances now appearing well distinguishable for all reported samples. A noticeable degree of structural order appears in the crystalline organization of all samples and definite decreases in the magnitude of coordination peaks entail intrinsic particle size effects.

Especially important here was the relationship resulting between Pt content and the reduction of the degree of lattice swelling in the presence of H_2. This fact, previously advanced on the basis of WAXS analysis, was substantiated by the results of Fig. 4: the contraction of the metal–metal distances, as the Pt content in the alloy increases, may be directly noted in Fig. 4 by following from the bottom the shifts of the peaks with respect to the bar used as a reference. The lattice parameter values, as

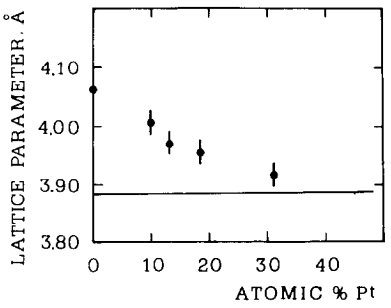

FIG. 5. Lattice parameter change of the PdPt hydride phases as a function of Pt alloyed. Full line indicates the PdPt alloy lattice constant as a function of Pt content (*30*).

TABLE 2

Structural Parameters

Catalyst	Lattice parameter[a] (Å)	Surface area, S_{sp}[b] (m^2/g)	$\bar{D}$[c] (Å)
Al 00	4.57	217	23
Al 10	4.01	142	31
Al 13	3.97	116	36
Al 18	3.95	146	28
Al 31	3.93	124	31
Al 100	3.91	119	24

[a] Under hydrogen flow.

[b] Per gram of alloy.

[c] Calculated using a spherical particle approximation from $\bar{D} = 3 \times 10^4/S_{sp}\,\rho$, where ρ is the alloy density.

calculated from the main coordination peak positions, are shown for all examined samples in column 1 of Table 2 and plotted in Fig. 5 vs the Pt atomic percentage in the metal phase.

Finally, Table 2 also gives the metal surface areas, S_{sp}, derived from SAXS measurements, together with mean particle dimensions, $\bar{D}$. Sample Al 13 appears less dispersed in agreement with the sharper details of the relevant radial curve.

DISCUSSION

From the data reported in the previous section it seems that our twofold object has been achieved: synthesis of alloy catalysts from support anchored organometallic species is a valuable method of preparing highly dispersed Pd/Pt clusters and, at the same time, specific formation of Pd/Pt alloys is demonstrated.

Organometallic species suitable for easy reduction to metal supply the ideal procedure for achieving fine metal dispersion; reduction of supported molecules generates single atoms from which the smallest metal particles are formed compatibly with support nature and experimental conditions, i.e., low temperature and a non-oxidizing atmosphere (*12, 17, 32, 33*). In attempting bimetallic synthesis, this procedure might

be severely restricted by the possibly different reactivity of the two supported organometallic precursors toward the reducing agent. In fact, the formation of bimetallic clusters from single atoms requires at least that suitable amounts of the two elements be produced at the same time. This condition appears fulfilled by the Pd(II) and Pt(II) allylic compounds coexistent on the support surface: in fact, their reduction with H_2 leads to alloy formation.

In this respect, it is noteworthy that alloy occurrence was observed in the whole range of composition explored: although literature on Pd/Pt systems is very scanty it is generally maintained that the two metals form an interrupted series of solid solutions (*34*), and our experimental results are in agreement with this. Moreover, our results are consistent with and supported by Chen and Schmidt (*35*) who ascertained fcc electron diffraction patterns for 20–200 Å diameter Pd/Pt alloy crystallites deposited by vacuum evaporation on planar amorphous SiO_2. Although our characterization mainly concerns PdPtH phases, it is well known that hydrides retain the structural organization of the parent metal or alloy lattices.

However, the clear appearance of PdPtH hydrides up to 31 at% Pt should be noticed. In fact Caga and Witterbottom (*11*) have recently reported that the addition of a Pt partner influences hydrogen solubility in Pd to the prevention of hydride phase formation at concentrations of 10–14.5 at% Pt. In the above work, mixed Pd–Pt oxide catalysts containing 0–15 at% were prepared and tested in hydrogenation of 1-octyne; the ability to form hydride phases was checked using methanol, *n*-hexane, and water as reduction media. The β hydride phase[1] occurrence was detected up to 5.6 at% Pt concurrent with simultaneous loss of activity. Above 10 at% Pt catalyst activity still declined with hydrogen pretreatment; but hydride phases were no longer observable. This absence was purported as reasonable grounds for supporting Pd/Pt alloy formation. Strictly speaking the lattice parameters of our catalysts indicated that β PtPdH formation is actually prevented at about 10 at% Pt, if the above-quoted constant $a_{Pd\beta} = 4.025$ Å is maintained as the lowest limiting value of the β phase lattice for the PtPdH system too. However, the trend shown in Fig. 5 is in contrast to a sudden disappearance of the hydride phases as a function of alloy composition. To this, beyond the very different treatment conditions used by Caga and Witterbottom, the dynamic process of formation of the hydride phase must be considered. The above authors refer to phases observed after prereduction times varying between 0.75 and 60 min, whereas we have recently reported that powder catalysts of Pd with analogous surface areas undergo phase changes in comparatively longer times (*19*).

Broadly, our results are more in keeping with those of Lewis (*28*), if catalyst Al 31 is momentarily disregarded. A continuous decline of hydrogen solubility has been reported which seems to be nullified within a range of compositions from 20 to 25% of Pt. Above about 10 at% Pt and 25°C the α and β phases coexist, but the limiting values of the lattice parameters characteristic of the α_{max} and β_{min} phases approach each other at the top of the miscibility gap. Moreover, for the hydrogen-richer side, it has also been stated (*28*) that minimum hydrogen contents at the β phase boundary diminish as a function of the Pt% content.

The pattern presented here agrees reasonably well with this frame and it might be safe to say that the hydride phases pertinent to Al 13 must be regarded as belonging to the two phases $\alpha + \beta$ PtPdH region.

Conversely, the appearance of hydride for sample Al 31 too is of great significance,

[1] Although β $PdH_{0.6}$ is used in (*11*) with reference to β palladium hydride as in a previous work (*36*), it is probable that the authors intended in (*11*) to refer to the β PtPd hydride phase.

as the hydrogen solubility gap is definitively closed at this Pt concentration. Several causes may concur to this result. A first possible explanation is that a substantial surface enrichment with Pd occurs in the alloy particles as foreseen by theoretical considerations (*37*) and put forward in some experimental works dealing with Pd/Pt alloy films (*8*). The observed hydride phase may concern an important superficial layer of unalloyed palladium, although our RDF's rather support the view that the "X-ray seen" metal particles are coherent domains of diffraction. It is also worth noting that, for highly dispersed Pd/Pt—SiO_2 catalysts, metal particle surface composition should not be substantially different from bulk composition, as has recently been pointed out (*7*).

A further argument may be put forward regarding the actual Pt alloyed in the Pt richer alloy, which may be less than the amount checked by plasma spectrograph analysis. If this is the case, an X-ray amorphous structural condition must be surmised for the separated portion of Pt; i.e., statistically distributed along the matrix. A bulk atomic arrangement would in fact give rise to asymmetries in the 111 profile reflections (see Fig. 2) or/and to a smearing of correlation peaks in the radial functions. Finally, and probably more pertinently, the divided state of metal phase cannot be disregarded in this comparison, previous results dealing with a massive metal form. From the results presented here, it is not easy to discriminate between the above hypotheses, all causes perhaps concurring in explaining behavior observed.

Despite this shortcoming, the performed characterization and behavior of catalysts under H_2 represent a sound frame for undertaking a catalyst study in hydrogenation reaction. It might be noted here that catalytic data are often used in assessing the formation of bimetallic clusters: on the contrary, we believe that the approach followed here is more appropriate in relating catalyst performance to alloy catalyst features.

ACKNOWLEDGMENTS

CNR, Rome, is acknowledged for financial support (Progetti Finalizzati-Chimica Fine e Secondaria).

REFERENCES

1. Sinfelt, J. H., *J. Catal.* **29,** 308 (1973).
2. Allison, E. G., and Bond, G. C., *Catal. Rev.* **7,** 233 (1973).
3. Ponec, V., *Catal. Rev.* **11,** 1 (1975); Sachtler, W. M. H., and Van Santen, R. A., "Advances in Catalysis and Related Subjects," Vol. 26. Academic Press, New York, 1977; Moss, R. L., and Whelley, L., Vol. 22. 1975; Gates, B. C., Katzer, J. R., and Schuit, G. C. A., "Chemistry of Catalytic Processes." McGraw-Hill, New York, 1979; Satterfield, C. N., "Heterogeneous Catalysis in Practice." McGraw-Hill, New York, 1980; Bassi, I. W., Garbassi, F., Vlaic, G., Marzi, A., Tauszik, G. R., Cocco, G., Galvagno, S., and Parravano, G., *J. Catal.* **64,** 405 (1980).
4. Graham, A. G., and Wanke, S. E., *J. Catal.* **68,** 1 (1981).
5. Wang, T., and Schmidt, L. D., *J. Catal.* **70,** 187 (1981).
6. Karpinski, Z., and Kòscielski, T., *J. Catal.* **56,** 430 (1979).
7. Karpinski, Z., and Kòscielski, T., *J. Catal.* **63,** 313 (1980).
8. Guczi, L., and Karpinski, Z., *J. Catal.* **56,** 438 (1979).
9. Moss, R. L., Pope, D., and Davis, B. J., *J. Catal.* **62,** 161 (1980).
10. Gomez, R., Fuentes, S., Fernandez Del Valle, F. J., Campero, A., and Ferreira, J. M., *J. Catal.* **38,** 47 (1975).
11. Caga, I. T., and Witterbottom, J. M., *J. Catal.* **57,** 494 (1979).
12. Carturan, G., Facchin, G., Cocco, G., Enzo, S., and Navazio, G., *J. Catal.* **76,** 405 (1982).
13. Ruiz-Vizcaya, M. E., Novaro, O., Ferreira, J. M., and Gomez, R., *J. Catal.* **51,** 108 (1978).
14. Grill, M., and Gonzales, R. D., *J. Catal.* **64,** 487 (1980).
15. Palazov, C., Chang, C. C., and Kokes, R., *J. Catal.* **36,** 338 (1975).
16. Lam, Y. L., and Boudart, M., *J. Catal.* **47,** 393 (1977); Yamaguchi, S., **50,** 541 (1977).
17. Cocco, G., Schiffini, L., Strukul, G., and Carturan, G., *J. Catal.* **65,** 348 (1980).
18. Palczewska, W., "Advances in Catalysis and Related Subjects," Vol. 24, p. 245. Academic Press, New York, 1975.
19. Benedetti, A., Cocco, G., Enzo, S., Pinna, F., and Schiffini, L., *J. Chim. Phys.* **78,** 875 (1981).
20. Carturan, G., and Gottardi, V., *J. Mol. Catal.* **4,** 349 (1979).
21. Benedetti, A., Cocco, G., Enzo, S., Piccaluga, G., and Schiffini, L., *J. Chim. Phys.* **78,** 961 (1981).

22. Cocco, G., Schiffini, L., Lucci, A., and Antonione, C., *J. Non-Cryst. Solids* **50,** 359 (1982).
23. Krogh-Moe, J., *Acta Crystallogr.* **9,** 951 (1956).
24. Cromer, D. T., and Mann, J. B., *Acta Crystallogr. A* **24,** 321 (1968).
25. Smith, V. H., Jr., Thakkar, A. J., and Chapman, D. C., *Acta Crystallogr. A* **31,** 391 (1975); Palinkas, G., and Radnai, T., **32,** 666 (1976).
26. Pings, C. J., and Waser, J., *J. Chem. Phys.* **48,** 3016 (1968).
27. Kratky, O., Pilz, I., and Schmitz, P. J., *J. Colloid. Interface Sci.* **21,** 24 (1966).
28. Lewis, F. A., "The Palladium–Hydrogen System." Academic Press, New York, 1967.
29. Baranowski, B., *in* "Topics in Applied Physics" (G. Alefeld and J. Wolkl, Eds.) Vol. 29. Springer-Verlag, Berlin, 1978.
30. Raub, E., and Worwag, G., *Z. Metallkd.* **46,** 513 (1955); Maeland, A., and Flanagan, T. B., *J. Phys. Chem.* **68,** 1419 (1964).
31. Urnes, S., *Phys. Chem. Glasses* **13,** 77 (1972).
32. Yermakov, Yu. I., *Catal. Rev.* **13,** 77 (1976).
33. Yermakov, Yu. I., Kuznetsov, B. N., and Zakharov, V. A., "Catalysis by Supported Complexes." Elsevier, Amsterdam, 1981.
34. Hansen, M., "Constitution of Binary Alloys," p. 1121. McGraw–Hill, New York, 1958.
35. Chen, M., and Schmidt, L. D., *J. Catal.* **65,** 198 (1979).
36. Caga, I. T., Shutt, E., and Winterbottom, J. M., *J. Catal.* **44,** 271 (1976).
37. Williams, F. L., and Nason, D., *Surf. Sci.* **45,** 377 (1974).